SUBMITTED 9 JUL 24
REVISION REQ. 21 AUG 24; REVISION RECD. 7 SEP 24
ACCEPTED 25 SEP 24
ONLINE-FIRST: OCTOBER 2024
DOI: https://doi.org/10.18295/squmj.10.2024.053

Biofilm-Induced Bone Degradation in Osteomyelitis

Insights from a comprehensive ex-vivo pathogen interaction study

***Ahmed Al Ghaithi,[1] John Husband,[2] Attika Al Bimani,[3] Mohammed Al Kindi,[3] Sultan Al Maskari[1]**

Departments of [1]Surgery, [2]Chemistry and [3]Microbiology & Immunology, Sultan Qaboos University, Muscat, Oman
**Corresponding Author's e-mail: a.alghaithi@squ.edu.om*

Abstract

Objectives: Osteomyelitis, marked by bone inflammation due to microbial infection, presents significant healthcare challenges. While the protective role of biofilm in bacterial immunity and persistence is well-documented, its direct impact on bone degradation in osteomyelitis remains inadequately characterized. This study aims to comprehensively examine the direct effects of biofilm-forming pathogens on human bone, providing new insights into the mechanisms of bone destruction in osteomyelitis. ***Methods***: Bone sections were collected from patients undergoing total knee replacement surgery between January 2021 and December 2022 for this study at Sultan Qaboos University Hospital. Then samples were inoculated with Staphylococcus aureus to simulate in-vitro bone infection. We then used Raman spectroscopy and Scanning Electron Microscopy (SEM) for detailed analysis of the bacterial interaction with bone tissue. ***Results***: SEM images depicted trabecular destruction caused by biofilm. Biofilm-forming pathogens contribute directly to bone exhibited by SEM images with marked trabecular destruction. Raman analysis showed a significant increase in the carbonate-phosphate ratio in inoculated samples (619%) compared to controls (47%). Mineral content decreased in inoculated samples, and the carbonate-to-amide I ratio reduced by 47% in inoculated and 80% in controls. The inoculated samples exhibited an 82% shift in collagen crosslinking compared to 72% in controls. ***Conclusion*:** This research enhances our

comprehension of the mechanisms behind bone destruction in osteomyelitis and underscores the intricate role of biofilm in the disease's development. These findings highlight the importance of biofilm in bone degradation and its potential implications for managing infections.
Keywords: Biofilm, Osteomyelitis, Bone and Bones, Raman Spectroscopy Microscopy, Electron, Scanning, Infection Control

Advances in Knowledge

- Using Raman spectroscopy and Scanning Electron Microscopy, we've unveiled direct impact of biofilm-forming pathogens on bone degradation in osteomyelitis.
- This knowledge challenges existing assumptions and could lead to more precise diagnostic and treatment strategies for osteomyelitis.

Application to Patient Care

- Our findings offer insights into the direct role of biofilm in bone deterioration, with potential implications for improving infection management approaches.

Introduction:

Osteomyelitis (OM) is an inflammatory condition of the bone caused by microbial infection, which can lead to bone necrosis and degradation. Typically, bones are sterile and resistant to bacterial colonization; however, trauma, surgery, or hematogenous spread of pathogens can compromise this integrity, resulting in infection[1]. Due to the varied manifestations of OM, many researchers have investigated its origins and developed systematic approaches for study, focusing on infection-related data such as blood tests, imaging, tissue examination, and bacterial cultures[2–4]. While some studies have examined the immune response's role in bone degradation, there has been limited focus on biofilm formation and its impact on bone damage[3].

Most OM pathogens can adhere to and proliferate on bone surfaces, joints, and implants, causing bone resorption. The precise mechanisms by which bacteria induce bone resorption remain unclear, though some evidence suggests that bacterial molecules on cell surfaces and secretions can trigger bone degradation[4]. Research has largely centered on the indirect effects of biofilms through host immune responses, with less attention on the direct impact of biofilm secretions on bone deterioration[3–6]. The biofilm hypothesis, proposed in 1978, posits

that bacteria can thrive in surface-bound communities, shielded from host defenses and antimicrobials[7–8]. This theory suggests biofilm-forming pathogens may directly damage tissues, although the clinical significance of direct bone resorption remains poorly understood.

Adam et al. proposed that virulent planktonic bacteria adhere to bone surfaces, form biofilms, and secrete extracellular matrices that promote bacterial adhesion, ultimately leading to bone cavitation and fragment detachment[3]. In chronic OM, avascular bone can harbor pathogenic biofilms, causing further bone lysis and cavitation[9].

This study aimed to explore the effects of biofilm-forming pathogens on human bone in an ex vivo setting, allowing us to investigate the impact without interference from the host immune response. This approach could enhance our understanding and inform more targeted OM treatments. Raman spectroscopy and Scanning Electron Microscopy were employed to achieve our research objectives.

Methods:

Preparation of Bone Samples:

The approval of the study was obtained from Medical Research & Ethics Committee of the College of Medicine & Health Sciences at Sultan Qaboos University (SQU-EC1039114) Bone sections were collected from patients undergoing total knee replacement surgery between January 2021 and December 2022 for this study. Informed written consent was obtained from all participants prior to sample collection. Sterile cancellous bone samples, measuring 1-2 cm^2, were meticulously cut using bone nibblers. These samples were then stored under sterile conditions in Normal Saline at a temperature of -20°C until the day of inoculation. Rigorous aseptic precautions were maintained throughout the entire process of bone sample handling. To ensure sterility, culture swabs were taken from the bone pieces and plated on blood agar medium for a 48-hour period just prior to processing. None of the samples displayed bacterial growth, nor did any of the patients develop subsequent infections.

Creation of Bacterial Inoculum:

A bacterial inoculum of Staphylococcus aureus was prepared from an overnight culture. A sterile solution of normal saline was mixed with the bacterial concentrate, resulting in concentrations ranging from 1 x 10^6 to 1 x 10^7 colony-forming units (CFU)/ml.

Subsequently, the bone samples were introduced into the bacterial mixture. As a control group, bone samples were immersed in sterile normal saline. Each mixture consisted of 12 bone pieces. The total of 24 samples were then incubated at 37°C to facilitate bacterial growth and proliferation. Every week, two bone samples from each mixture were selected for examination. Following the examination, the samples were disposed of in accordance with the established protocols for human tissue disposal at our hospital.

Examination of Bacterial Growth and Bone Resorption:

Scanning Electron Microscopy Setup:

The bone samples were fixed in Karnovsky's Electron Microscopy fixative, a solution containing 2.5% glutaraldehyde at pH 7.2, for a duration of 4 hours. Afterward, they were washed twice with a washing buffer for 10 minutes each time. The samples were then post-fixed using 1% osmium tetroxide for an hour, followed by a dehydration process using various concentrations of ethanol (25%, 75%, 95%, and 99.9%). The dried samples were mounted on aluminium stubs using Autosamdri-815® (Rockville, MD, USA), and subsequently coated with a layer of gold using the BioRad SEM coating system. Micrographs were obtained using a JEOL JSM-5600LV scanning electron microscope (JEOL Ltd, Tokyo, Japan).

Raman Spectroscopy Setup:

Raman spectra of the bone samples were acquired using a Raman spectrometer (I-Raman Ex spectrometer, BWTek, Newark, USA) equipped with an excitation laser diode operating at 1064nm. Spectra were recorded within the range of 400-2000 $cm^{-1.}$

Analysis of Spectra:

The obtained spectra were analysed using BWSpec® software (BWTek, Newark, USA). This software facilitated automated baseline correction and signal averaging to enhance signal-to-noise ratios. Key Raman bands were manually identified, and the impact of the bacterial osteolytic process on various aspects of bone composition, including mineral content, carbonate content, collagen cross-linking, and mineral and collagen fibril orientation, was studied.

Statistical Analysis:

Statistical analysis of Raman parameters from inoculated bone samples was compared to the control group using Statistical Package for the Social Sciences 2016 (SPSS) (IBM Corporations, New York- USA). This analysis aimed to determine any alterations in the ultrastructure of the examined bone architecture. The threshold for significance was set at a P value of < 0.05, and a Paired T-test was employed.

Results:

Isolation of bacteria from analysed surfaces:

Bacterial biofilms that grew under the conditions described in the Methods section were successfully isolated from the surfaces of the examined samples using swabs. These swabs were cultured in blood agar medium for a duration of 48 hours. Over eight consecutive weeks, cultured swabs from the inoculated samples showed positive results, in contrast to the negative cultures from the control samples. The average bacterial count in the agar dishes was measured at 5×10^5 CFU/ml.

Raman spectrometry analysis:

Utilizing Raman spectrometry, we conducted a comprehensive study of the micro-architectural changes in the bone. The standard bone spectrum demonstrated distinct peaks for phosphate (958 cm^{-1}) and carbonate (1070 cm^{-1}) in Figure 1A. The Raman bands at 851, 873, and 917 cm^{-1} were indicative of the collagen and hydroxyproline matrix, while the band at 1001 cm^{-1} was characteristic of phenylalanine. The band ranging from 1210 to 1320 cm^{-1} corresponded to amide III. Figure 1B displayed the average Raman spectra collected from both the control and inoculated samples after eight weeks of incubation.

The ratio of carbonate to phosphate serves as an indicator of bone mineral content, which notably increased over time in the inoculated bone samples compared to the control group. This points to a change in bone crystallinity, shifting from a hard matrix to a brittle one. The control group's mean values ranged from 0.19 to 0.28 across different weeks, while inoculated samples showed ratios varying from 0.21 to 1.51. In week 8 the increase in ratio was significant at 61.9% in the inoculated samples, compared to 47% in the controls ($P > 0.05$, figure 2A).

A progressive reduction in mineral content was observed in the inoculated samples when compared to the control group. Phosphate-to-amide ratios in control samples varied over weeks, peaking at week one (13.87) and dropping at week eight (6.25). Inoculated samples followed a similar pattern, with the highest ratio at week one (13.20) and the lowest at week eight (2.39). While the inoculated samples experienced an 82% reduction, the control group showed a 55% reduction at week 8. However, this difference was not statistically significant ($P < 0.05$, figure 2B).

Control samples demonstrated variable carbonate-to-Amide I ratios, spanning from 0.04 to 0.0214 across the eight weeks. Inoculated samples also showed variation, with values ranging from 0.06 to 0.0119 at week 8. The inoculated samples experienced a 47% reduction in these ratios, whereas the control group exhibited an 80% reduction. However, the difference was not statistically significant ($P < 0.05$, figure 2C).

The organic composition of the examined bone samples was assessed using the ratio of amide I Raman band at 1660 cm^{-1} to 1668 cm^{-1}. Mean ratios in control samples ranged from 3.89 to 1.09 across different weeks, while inoculated samples displayed varying ratios from 3.149 to 0.56. An 82% shift in the amide band was observed in the inoculated samples compared to 72% in the control group. However, this difference was not statistically significant ($P < 0.05$, figure 2D).

Scanning Electron Microscopy results:

In the critical stages of the sixth and eighth weeks of our experimental timeline, a significant juncture was reached with the meticulous examination of bone samples utilizing scanning electron microscopy (SEM). The SEM images unveiled a striking divergence between the control and inoculated groups. In the control samples, the SEM images showcased the characteristic appearance of cancellous bone, reminiscent of a honeycomb structure. This familiar honeycomb trabecular pattern is a hallmark of healthy bone tissue and was faithfully preserved in the control group. Conversely, the images from the inoculated specimens revealed a profoundly altered landscape. Within these samples, the SEM unveiled a stark departure from the organized trabecular architecture seen in the control samples. Instead, a remarkable destruction of the trabeculae was observed. The detrimental impact of the Staphylococcus aureus biofilm on the bone's internal structure was readily apparent. Furthermore, the SEM examination allowed for a comprehensive analysis across various

magnification levels. These different magnifications accentuated the extent of the trabecular destruction caused by the biofilm. Figure 3 serves as a poignant representation of these observations.

Discussion:

This study revealed discernible cavitation and disruption within the examined bone samples, a phenomenon that was evident through the employed SEM. The outcomes of this experimental investigation underscored the capacity of pathogenic biofilm to directly trigger bone resorption, mirroring the clinical scenarios encountered in cases of osteomyelitis. Notably, the efficacy of Raman spectroscopy in detecting these structural alterations was also demonstrated.

All inoculated bone samples subjected to Raman testing exhibited noteworthy quantitative and qualitative ultrastructural deterioration induced by the biofilm, distinguishing them from the control samples. The selection of Raman spectroscopy was based on its ability to meticulously analyse molecular changes within materials at an ultrastructural level.[12,17] Notable differences between the two groups emerged in later time points, particularly in factors like the phosphate-to-amide I ratio, carbonate-to-amide I ratio, and amide 1660-to-1668 ratio. However, the pivotal finding remains that bacterial biofilm was accompanied by marked and noteworthy bone degradation, particularly evident in the initial weeks. As the experiment progressed, it is conceivable that bacterial counts began to decline due to dwindling nutrient availability in the media, potentially leading to a reduction in osteolytic activity during the later stages. Similar outcomes are observed when examining non-healthy bone samples, indicating a deterioration in the ultrastructural composition of the bone.[17,18] Furthermore, this study highlights the fact that the occurrence of biofilm formation is not limited solely to chronic osteomyelitis, as previously elucidated by Adam J et al. Their comprehensive experiment unveiled the ability of diverse bacterial strains, to effectively cultivate mature biofilms within a mere seven-day timeframe across various substrate surfaces. Notably, this formation of biofilm was noticed regardless of the specific culture media used for growing them, highlighting the strength and adaptability of these biofilm structures. [5] This understanding emphasizes the necessity for carefulness in handling acute infections, revealing the likelihood of biofilm formation in the early stages of the disease. It underscores the complexities posed by biofilm structures, where bacteria within biofilms exhibit antibiotic resistance levels ranging from 10 to 1000 times higher than their planktonic

counterparts. [16] This strategy is particularly crucial when managing infected surgical wounds that involve metallic implants, as the decision to retain or remove the implant presents a challenging dilemma. The presence of a biofilm on the implant surface can lead to persistent infection and compromised healing, necessitating a comprehensive approach to disrupt the biofilm and prevent its reformation.[4,19]

A primary and highly effective approach for addressing biofilm infections revolves around physical removal, coupled with inhibiting biofilm reconstitution. Therefore, establishing an effective management approach for bone infection necessitates exploring into the etiopathogenesis of the biofilm formation. This entails acquiring a comprehensive understanding of the complex molecular interactions that transpire not only among bacteria themselves but also between bacteria and the host. The process of biofilm formation is generally categorized into four primary stages[19,20]: initial bacterial attachment to a surface, subsequent microcolony development, then progression towards biofilm maturation, and eventual detachment, often referred to as dispersal. This detachment enables the released bacteria to potentially colonize new surfaces and areas.[20]

This is why, to enhance efforts of addressing the biofilm, novel strategies are being investigated targeting these formation stages. These encompass preventing initial bacterial attachment to surfaces, disrupting cell-to-cell signaling pathways, utilizing bacteriostatic or bactericidal agents, and exploring the potential of anti-biofilm materials while using implants. These emerging tactics hold substantial promise in addressing the complexities posed by biofilm infections, offering the potential for more targeted and efficacious treatment strategies. As an illustration, Caluss M. et al conducted a prospective nonrandomized comparative study that encompassed 135 cases of lesser toe deformities. Their investigation involved analyzing biofilm-related infections using sonication. The findings revealed a diminished biofilm formation (load) on titanium K wires in contrast to stainless steel K wires. Furthermore, employing titanium K wires yielded improved clinical outcomes compared to their stainless-steel counterparts.[21]

Conclusion:

This research enhances our comprehension of the mechanisms behind bone destruction in osteomyelitis and underscores the intricate role of biofilm in the disease's development.

These findings highlight the importance of biofilm in bone degradation and its potential implications for managing infections.

Authors' Contribution

AG and JH contributed to developing the project idea, helped interpret the results and prepared and revised the manuscript. AB and MK contributed to idea development, data collection, preparation and revising the manuscript. SM contributed to developing the idea and critically revising the manuscript. All authors approved the final version of the manuscript.

Conflict of Interest

The authors declare no conflicts of interest.

Funding

Open Access funding provided by Oman National Research Council, Muscat, Oman.

Data Availability Statement

All data generated in the current study are available from the corresponding author on reasonable request**.**

References:

1. Kavanagh N, Ryan EJ, Widaa A, Sexton G, Fennell J, O'Rourke S, et al. Staphylococcal Osteomyelitis: Disease Progression, Treatment Challenges, and Future Directions. Clin Microbiol Rev. 2018 Apr;31(2). doi: 10.1128/CMR.00084-17.

2. Norden CW. Lessons learned from animal models of osteomyelitis. Rev Infect Dis. 1988 Feb;10(1):103–10. PMID: 3282645.

3. Al Farii H, Zhou S, Albers A. Management of Osteomyelitis in Sickle Cell Disease: Review Article. J Am Acad Orthop Surg Glob Res Rev. 2020 Sep;4(9):e20.00002-10. doi: 10.5435/JAAOSGlobal-D-20-00002. PMID: 32890008; PMCID: PMC7470010.

4. Hashmi, A. Z. A., Fazari, E. A., Ward, M. A., Masruri, R. A., Balushi, S. A., Mutani, M. A., Ghaithi, A. A., & Baluki, W. A. (2024). Predictors of Developing a Complex Course of Osteomyelitis in Patients with Sickle Cell Anaemia. *Sultan Qaboos University medical journal*, *24*(1), 58–62. https://doi.org/10.18295/squmj.12.2023.083

5. Junka A, Szymczyk P, Ziółkowski G, Karuga-Kuzniewska E, Smutnicka D, Bil-Lula I, et al. Bad to the Bone: On In Vitro and Ex Vivo Microbial Biofilm Ability to Directly Destroy Colonized Bone Surfaces without Participation of Host Immunity or Osteoclastogenesis. PloS One. 2017;12(1):e0169565. doi: 10.1371/journal.pone.0169565.

6. Khalid, M., Bora, T., Ghaithi, A.A. *et al.* Raman Spectroscopy detects changes in Bone Mineral Quality and Collagen Cross-linkage in Staphylococcus Infected Human Bone. *Sci Rep* **8**, 9417 (2018). https://doi.org/10.1038/s41598-018-27752-z

7. Young AB, Cooley ID, Chauhan VS, Marriott I. Causative agents of osteomyelitis induce death domain-containing TNF-related apoptosis-inducing ligand receptor expression on osteoblasts. Bone. 2011 Apr 1;48(4):857–63. doi: 10.1016/j.bone.2010.11.015.[4]

8. Nair SP, Meghji S, Wilson M, Reddi K, White P, Henderson B. Bacterially induced bone destruction: mechanisms and misconceptions. Infect Immun. 1996 Jul;64(7):2371–80. PMID: 8698529.

9. Khalil H, Williams RJ, Stenbeck G, Henderson B, Meghji S, Nair SP. Invasion of bone cells by Staphylococcus epidermidis. Microbes Infect. 2007 Apr;9(4):460–5. doi: 10.1016/j.micinf.2007.01.011.

10. Morris MD, Mandair GS. Raman assessment of bone quality. Clin Orthop. 2011 Aug;469(8):2160–9. doi: 10.1007/s11999-010-1739-0.

11. Gong B, Morris MD. Raman spectroscopy monitors adverse bone sequelae of cancer radiotherapy. Chin Chem Lett. 2015 Apr 1;26(4):401–6. doi: 10.1016/j.cclet.2014.12.015.

12. Stoodley P, Ehrlich GD, Sedghizadeh PP, Hall-Stoodley L, Baratz ME, Altman DT, et al. Orthopaedic biofilm infections. Curr Orthop Pract. 2011 Nov;22(6):558–63. doi: 10.1097/BCO.0b013e3182356ca2.

13. Lee K-J, Goodman SB. Identification of periprosthetic joint infection after total hip arthroplasty. J Orthop Transl. 2015 Jan 1;3(1):21–5. doi: 10.1016/j.jot.2014.10.002.

14. Del Pozo JL, Patel R. Infection Associated with Prosthetic Joints. N Engl J Med. 2009 Aug 20;361(8):787–94. doi: 10.1056/NEJMra0803502.

15. Cassat JE, Hammer ND, Campbell JP, Benson MA, Perrien DS, Mrak LN, et al. A secreted bacterial protease tailors the Staphylococcus aureus virulence repertoire to modulate bone remodelling during osteomyelitis. Cell Host Microbe. 2013 Jun 12;13(6):759–72. doi: 10.1016/j.chom.2013.05.003.

16. Al Ghaithi A, Al Bimani A, Al Maskari S. Investigating the Growth of Pseudomonas aeruginosa and Its Influence on Osteolysis in Human Bone: An In Vitro Study. Strategies Trauma Limb Reconstr. 2021 Sep-Dec;16(3):127-131. doi: 10.5005/jp-journals-10080-1534.

17. Al-Ghaithi A, Husband J, Al-Maskari S. Analysis of Bone Microarchitectural Changes and Structural Damage in Sickle Cell Disease-Induced Avascular Necrosis Using Raman Spectroscopy: Is there potential for medical management? Sultan Qaboos Univ Med J. 2021 May;21(2):e297-e301. doi: 10.18295/squmj.2021.21.02.020.

18. Shen J, Fan L, Yang J, Shen AG, Hu JM. A longitudinal Raman microspectroscopic study of osteoporosis induced by spinal cord injury. Osteoporos Int. 2010;21:81–7. doi: 10.1007/s00198-009-0949-3.

19. Penesyan, A., Nagy, S.S., Kjelleberg, S. et al. Rapid microevolution of biofilm cells in response to antibiotics. npj Biofilms Microbiomes 5, 34 (2019). doi: 10.1038/s41522-019-0108-3.

20. Crouzet, M., Le Senechal, C., Brözel, V.S. et al. Exploring early steps in biofilm formation: set-up of an experimental system for molecular studies. BMC Microbiol 14, 253 (2014). doi: 10.1186/s12866-014-0253-z.

21. Clauss, M., Graf, S., Gersbach, S., Hintermann, B., Ilchmann, T., & Knupp, M. (2013). Material and biofilm load of K wires in toe surgery: titanium versus stainless steel. Clinical orthopaedics and related research, 471(7), 2312–2317. doi: 10.1007/s11999-013-2882-7.

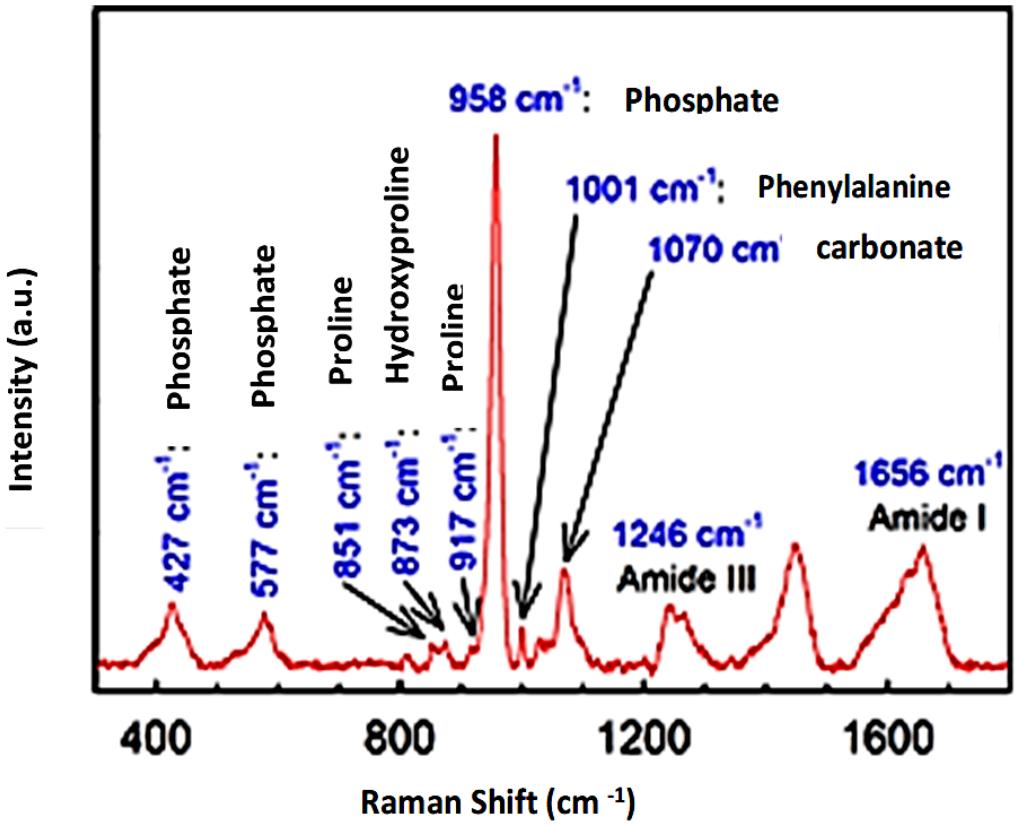

A

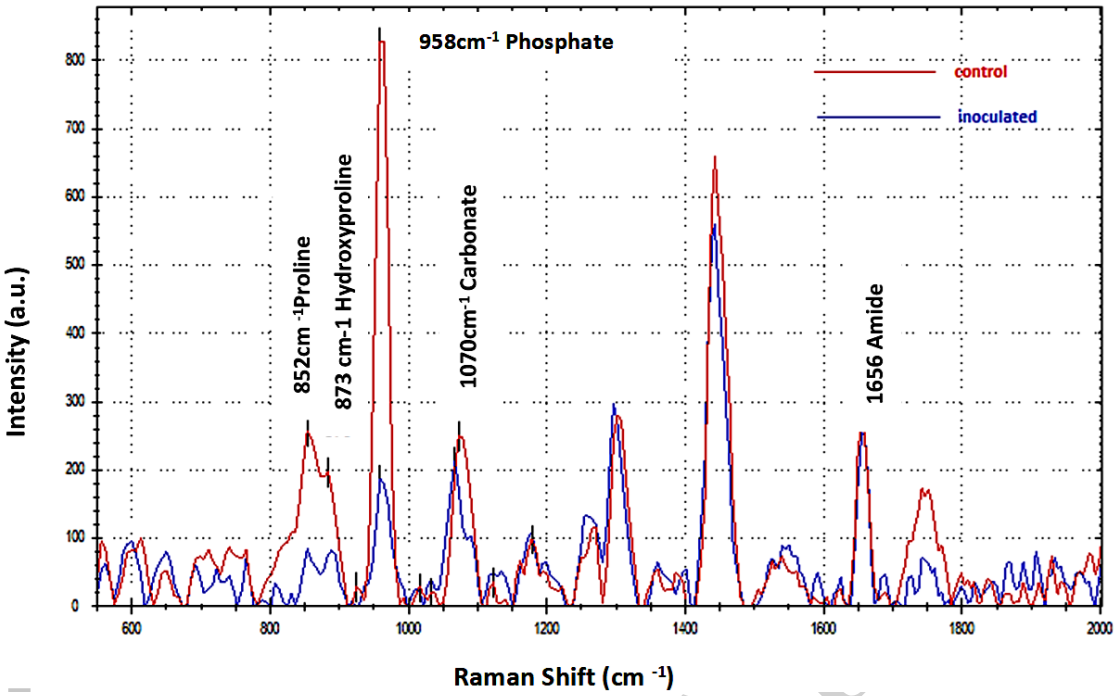

353 B

354 **Figure 1**: **A**: Typical Raman spectrum of healthy human bone with labelled waves' peaks of
355 interest. **B**: Average Raman spectra collected from both control and inoculated samples at
356 eight weeks of incubation.

357

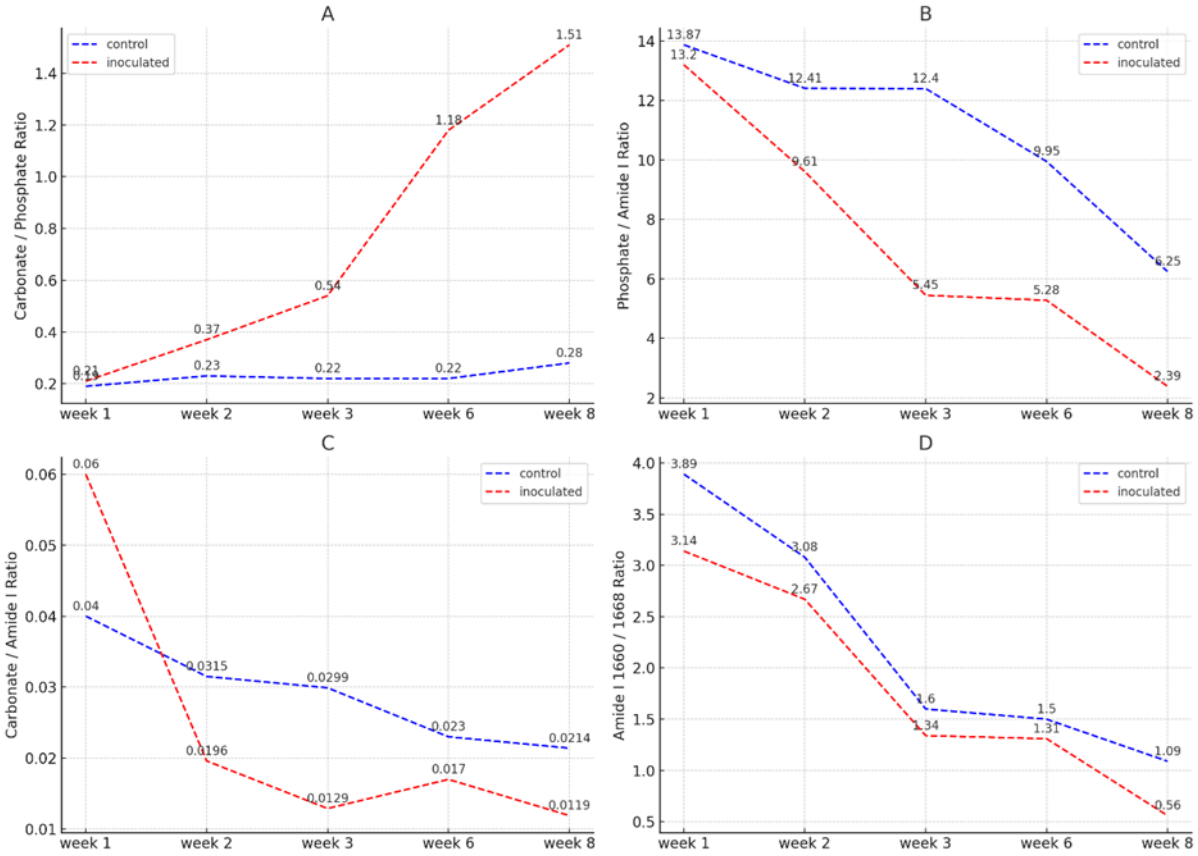

Figure 2: (**A**) Shows an increase in carbonate to phosphate ratio in inoculated samples compared to controls indicating changing bone crystallinity and transformation to a brittle matrix. (**B&C**) shows the reduction in mineral content relative to the organic material in inoculated samples compared to controls. (**D**) collagen crosslinking ratio shown as shift of the Raman bands at 1660cm^{-1} to 1668 cm^{-1} in inoculated samples compared to controls representing the destruction of collagen cross linkage.

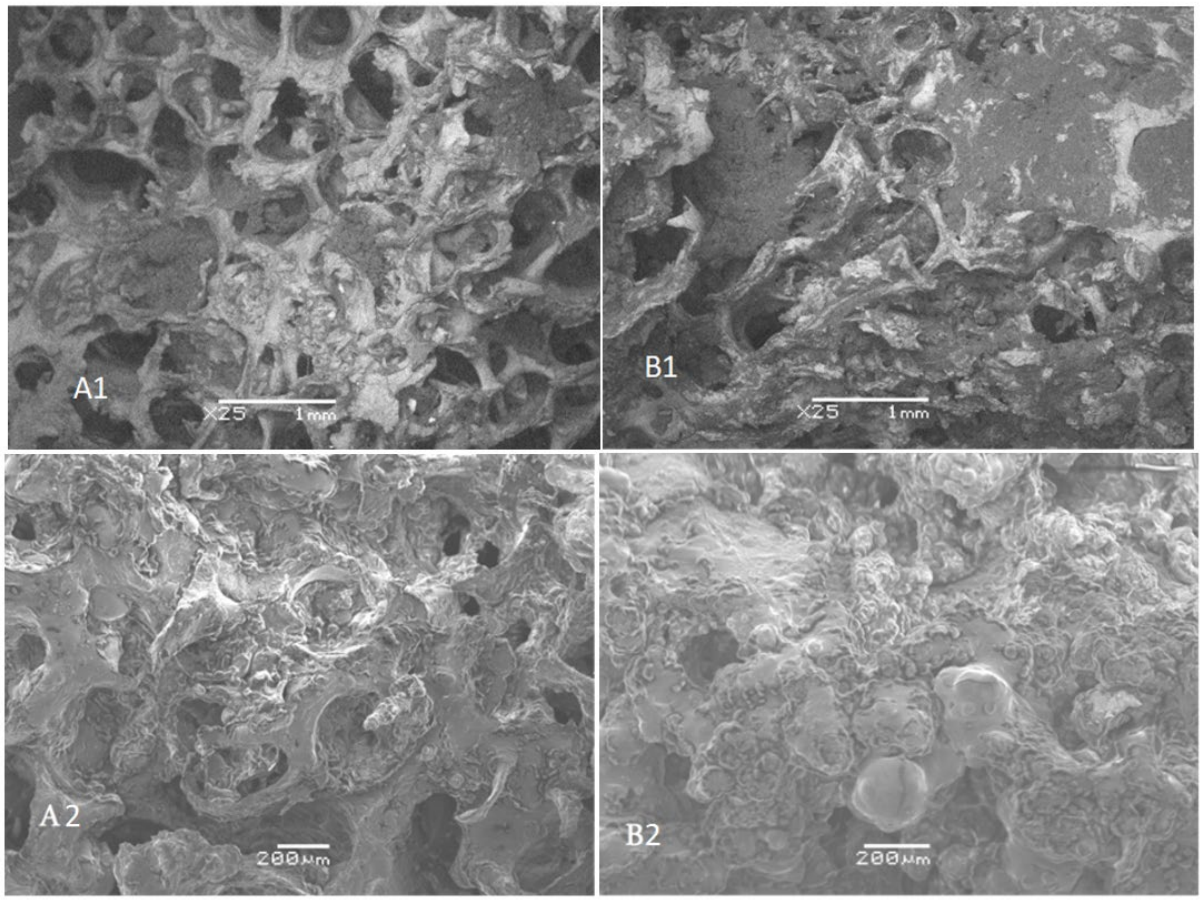

366

367 **Figure 3**: SEM images showing a divergence between the control and inoculated groups.